energies

MDPI

*Article*

# Oil-Removal Performance of Rotating-Disk-Type Oil Separator

**Haneol Lee, Yeawan Lee, Yong-Jin Kim, Bangwoo Han and Hak-Joon Kim ***

Department of Sustainable Environment Research, Korea Institute of Machinery & Materials, Daejeon 34103, Korea
* Correspondence: diayolk@kimm.re.kr; Tel.: +82-42-868-7775; Fax: +82-42-868-7284

**Abstract:** Oil mist adversely affects the health of workplace workers, and for this reason, regulations on the limitation of the oil-mist exposure of workers are becoming stricter. In order to reduce the amount of the exposure of workers to oil mist, it is important to effectively remove oil mist from machine tools. In this study, the collection efficiency according to the geometry of the oil-mist-collection cyclone consisting of several disks and the output power and rotation speed of the motor were evaluated. Most of the generated oil mists were less than 10 μm, and the mist removal was assessed using an optical particle counter. The cyclone airflow rate increased linearly with the rotational speed, and the rate was affected more by the cyclone geometry than by the power consumption. The mist-removal performance was significantly enhanced when plate- and cone-type disks were added to the rotating blades. The removal efficiencies of $PM_{10}$ and $PM_{2.5}$ under the maximum operational conditions of 5000 rpm and a flow rate of 3.73 $m^3$/min were 93.4% and 78.4%, respectively. The removal capacity was more affected by the cyclone geometry than the rotational speed. The experimental results were similar to those predicted by the modified Lapple theory when an appropriate slope parameter ($\beta$) was used.

**Keywords:** oil mist; centrifugation; cyclone; metalworking fluid



**Citation:** Lee, H.; Lee, Y.; Kim, Y.-J.; Han, B.; Kim, H.-J. Oil-Removal Performance of Rotating-Disk-Type Oil Separator. *Energies* **2022**, *15*, 6515. https://doi.org/10.3390/en15186515

Academic Editor: Keiichiro Yoshida

Received: 19 May 2022
Accepted: 2 September 2022
Published: 6 September 2022



## 1. Introduction

Metalworking fluids (MWFs) improve metal working, prevent workpiece corrosion, extend the tool life, and improve the processing accuracy by removing heat and chips that are generated during metal cutting [1–3]. However, MWFs generate oil mist because of the evaporation that occurs under the high cutting temperatures of metalworking processes, dispersion attributable to the high-speed rotation of the cutting tool and workpieces, and atomization caused by the impact of the fluid on the cutting tool, workpieces, and machine [4–8].

Oil-mist emissions during machining increase the airborne-particle concentration of the working environment. Oil mist poses an occupational health risk, and it is associated with skin inflammation, laryngeal cancer, asthma, and bronchial hyper-responsiveness. As such, because exposure to MWF oil mist adversely affects the health of workers, regulations on the exposure to MWF oil mist have been established. The final report of the Occupational Safety and Health Administration (OSHA) Metalworking Fluids Standards Advisory Committee, published in 1999, recommends new 8 h time-weighted average permissible exposure limits (PEL) of 0.4 mg/$m^3$ thoracic particulate (0.5 mg/$m^3$ total particulate) [9]. Similarly, in South Korea, the government stipulates a workplace worker's oil-mist-exposure limit of 0.8 mg/$m^3$ based on the time-weighted average (TWA), and it requires employers to operate an exposure and health monitoring system for workers exposed to hazardous substances [10]. However, the long-term exposure of workers to oil mist, even at concentrations lower than the abovementioned limits, also induces upper and lower respiratory symptoms in workers [11]. Therefore, it is important to control the oil-mist concentration in the workplace to reduce the amount to which workers are exposed.

In order to reduce the exposure of workers in the workplace to oil mist, the OSHA recommends the use of appropriate personal protective equipment, engineering and work-practice controls, and administrative controls. Engineering and work-practice controls include the proper design and operation of the MWF delivery system, effective local exhaust ventilation, effective general or dilution ventilation, and the proper maintenance of equipment [12]. Wearing personal protective equipment, such as a dust mask, can help reduce the worker exposure to oil mist [13,14]. Typically, the N95/R95/P95-grade masks of the United States have a filtration efficiency of 95% and are the most commonly used masks to protect the respiratory tract from polluted particles in the industrial workplace [15,16]. However, the higher the filtration efficiency of the mask, the greater the respiratory resistance, which may cause the amplification of respiratory fatigue due to the increase in respiratory resistance, and a decrease in the physical-work ability. In addition, the prolonged and continuous use of the mask can cause lung injury [17–21]. For this reason, it is important to wear personal protective equipment, but it is also important to reduce the concentration of oil mist in the workplace.

In general, oil-mist particles generated by machine tools have a diameter of $\geq$1 μm [7]. Many studies have investigated factory-oil-particle concentrations and size distributions. Chen et al. [8] studied the mist-particle size distribution and worker exposure during the forming, threading, and heat treatment of fasteners. The mass median aerodynamic diameter of the coarse-mode particles ($d_{ae}$ > 3.5 μm) ranged from 8.16 to 13.0 μm [8]. Sokolović et al. [22] studied oil mist generated from oil-in-water MWF emulsions at three different concentrations. The particle diameter ranged from 0.3 to 12.5 μm. Sutherland et al. [23] measured the concentration and size distribution of particles generated in a closed computer-numerical-control (CNC) lathe under wet and dry cutting conditions. When high-speed dry machining was in progress, most of the particles generated were 1–4 μm in diameter during wet machining, and the diameter was <1 μm. Wang et al. [1] studied the oil-mist-emission rates during milling, and most of the particles were from 1.8 to 12.5 μm in diameter.

A ventilation system is used to purify the air inside the work area without being directly connected to a mist-generating source. It has the advantage that it can be applied even when the machine tool does not have an enclosure. Due to the large size of the ventilation system, it takes up a lot of installation space and cost, and proper airflow must be maintained to efficiently remove the mist or workers may still be exposed to high concentrations of mist at the source [24]. Therefore, a more efficient treatment of fine oil mists and fumes in machine-tool workshops is required [25]. Various air-purification devices, including gravitational settling, wet scrubbers, centrifugal oil-mist collectors, fabric filters, and electrostatic precipitators (ESPs), have been used. Gravitational settling is the simplest method to remove suspended particles from airflow. A gravitational-settling system is inexpensive, easy to install and maintain, and has a low-pressure drop, but its use is limited because it is only effective for very large particles [26]. A wet scrubber removes contaminants by spraying water from the top of the tower with a total water flow large enough so that the cross section of the drip curtain "covers" the entire aerosol flow in the opposite direction for efficient operation. In addition, there is the disadvantage that a system capable of treating water containing polluted substances is required [26].

Oil-mist filtration by fibrous media is commonly used in many industrial applications [27,28]. Fiber filters have been widely used to remove oil mists due to their small pore size, large surface area, well-interconnected pores, and flexibility [28]. The pressure drop and filtration efficiency according to the energy consumption are the most important variables to evaluate the filtration performance of fiber filters [29]. Many studies have been conducted on the factors that affect the filtration performance of fiber filters. For example, research is underway to improve the filter performance through the filter media parameters, fabric layout, the fabrication of nanofiber filter media, and filter-surface modification [30–32]. Filtration systems that use HEPA filters can effectively remove even submicron particles. However, over time, the blowing efficiency may fall, which is attributable to the differential pressure caused by clogging (the mist adheres to the filter) [33].

With the long-term use of filters in environments with high mist levels, the filters can cause bad odors and frequent filter replacement is required. However, this is costly and affects productivity because production must sometimes be paused [33]. Moreover, the waste filters are secondary pollutants, and thus the existing oil-mist collectors are suboptimal.

ESPs have a low-pressure drop because they do not use a filter. In addition, the airflow does not decrease over time, and the collection efficiencies remain high if the collection plate is cleaned regularly, which is economical. However, the collection efficiency of ESPs is affected by many factors, including the relative humidity, air temperature, and dust-collector geometry [34–38]. However, the efficiency steadily decreases until cleaning is performed, and an electric arc may develop if metal dust or chips are collected. Moreover, ozone is generated due to corona discharge, and a water-soluble MWF is not recommended because of the electrical leakage.

The centrifugal oil-mist collector is the oldest oil/coolant mist-collection technology on the market. A pressure differential between the inside and outside of the device is created by the rotating drum, and mist-laden air is drawn into the device. As the name implies, oil-laden air moves outward from the center of the drum by centrifugal force. This oil-laden air is captured by a sponge-foam-type filter attached to the outside of the drum. As the device is used, the sponge-foam-filter pad saturates quickly, which reduces the airflow and the amount of mist it can handle, resulting in reduced efficiency and the mist escaping from the machine enclosure into the air [39]. A clogged filter can also create an unbalanced condition as the unit rotates, which often results in severe vibrations. These vibrations can be transmitted to the machine tool and cause part-quality problems [39]. Both water-soluble and water-insoluble metalworking fluids can be treated when the centrifugal oil-mist collector is used. However, because of the use of filters, it still requires periodic filter replacement.

In this study, an oil collector was developed in which the filter was replaced with several disks. This oil-mist collector uses centrifugal force as an operating principle, similar to the conventional centrifugal oil-mist collector. However, this study tried to increase the processing efficiency by using multiple disks instead of filters. Oil-laden air passes through a rotor with a large number of cone-shaped disks, which are stacked with small gaps but have gas-passage openings near the axis of rotation. The particles near the rotor axis are radially accelerated by the centrifugal force and thereby contact the cone-shaped inner surfaces of the nearest disks, where they agglomerate into larger droplets and wall films. They then separate into larger droplets at the edges of the disks and flow along the inner wall of the casing to the oil outlet. Gas with reduced oil mist is exhausted along the inner wall of the cyclone. The disk performance was evaluated by testing in the absence of a disk, and in the presence of flat and cone-shaped disks. Two rotors and three motors were evaluated, and the oil-removal efficiency and capacity were quantitatively analyzed according to the power consumption, rotor diameter, and rotational speed. The test results were compared with a commercial centrifugal oil-mist collector. Finally, the removal efficiencies of oil particles of varying diameters were compared with those predicted by the modified Lapple theory.

## 2. Materials and Methods

Figure 1 shows the three rotating-disk cyclones used in this study. Each disk cyclone has a rotor blade that sucks in air, and disks or cones placed at equal intervals at the edge of the blade, as well as a motor. The rotational speed (revolutions per minute (rpm)), air velocity through the gaps between the disks or cones, suction flow rate, and mist-removal efficiency, as the rotor blade height and length, disk shape and size, and motor power changed, were evaluated.

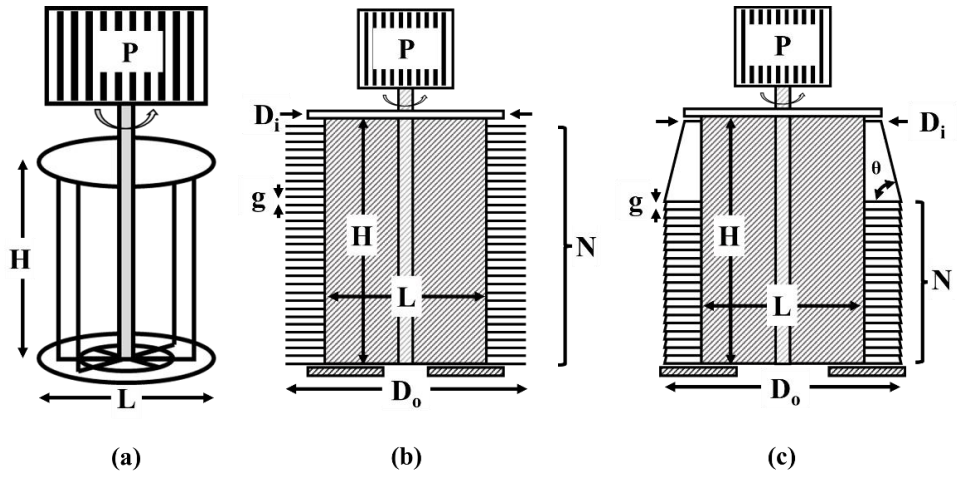


**Figure 1.** Schematic of the cyclone separator: (**a**) no disks attached; (**b**) flat disks attached; (**c**) cone-shaped disks attached.

Figure 1a shows a device equipped with a rotary blade that sucks in polluted air as the blade rotates. Figure 1b shows a flat circular disk mounted on the edge of the rotor blade, which delivers a strong centrifugal force to the air being sucked in. Figure 1c shows a rotating-type cyclone in which a downward cone-shaped disk is attached to the rotor, which increases the centrifugal force and air-residence time.

Figure 2 shows rotating cyclones in which the sizes and lengths of the rotor blades, inner and outer diameters of the cone disk, and rotational power vary. Table 1 summarizes the geometry, size, and power of the rotating-disk cyclones shown in Figures 1 and 2.

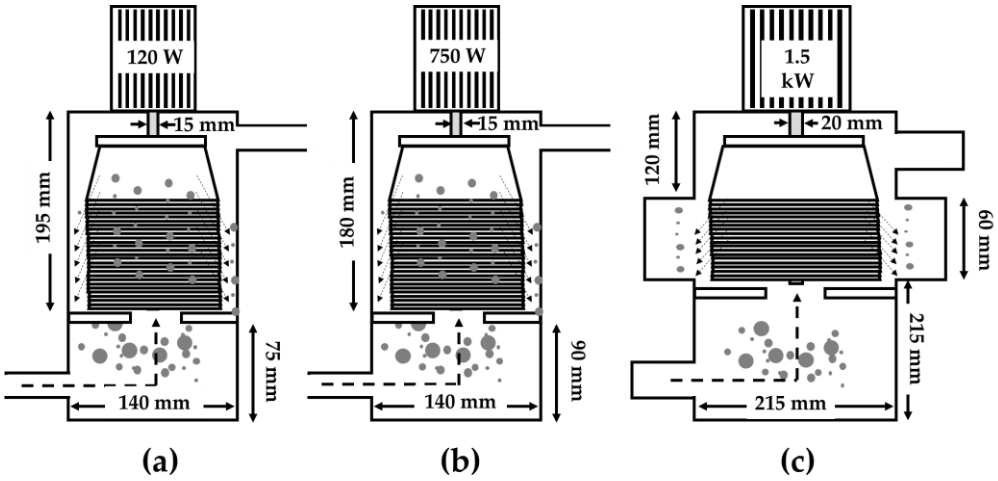


**Figure 2.** Schematic of a disk-stack centrifugal cyclone separator: (**a**) cyclone with 120 W motor, (**b**) cyclone with 750 W motor, (**c**) cyclone with 1.5 kW motor.

**Table 1.** Dimensions of the experimental cyclones.

| Case | Disk Type | Propeller Height (H, mm) | Propeller Length (L, mm) | Cone Angle (θ, °) | Disk Inner Diameter ($D_i$, mm) | Disk Outer Diameter ($D_o$, mm) | Disk Gap (g, mm) | Rotating Motor Power (P, W) | Number of Stacks (N, #) |
|---|---|---|---|---|---|---|---|---|---|
| 1 | none | 120 | 80 | none | none | none | none | 120 | none |
| 2 | flat | 120 | 80 | 0 | 80 | 115 | 3 | 120 | 20 |
| 3 | cone | 120 | 80 | 30 | 80 | 115 | 3 | 120 | 20 |
| 4 | cone | 120 | 80 | 30 | 80 | 115 | 3 | 750 | 20 |
| 5 | cone | 133 | 130 | 30 | 130 | 185 | 3 | 1500 | 20 |

Figure 3a shows an operational schematic of the cyclone in this study. Given the pressure difference between the inside and outside of the cone-shaped disks as the blade rotates, air flows from the inlet to the bottom of the separator. The working principle of the disk-stack cyclone separator is based on centrifugal force. Oil-laden air passes through a rotor with a large number of cone-shaped disks, which are stacked with small gaps but have gas-passage openings near the axis of rotation. The particles near the rotor axis are radially accelerated by the centrifugal force and thus contact the cone-shaped inner surfaces of the nearest disks, where they agglomerate into larger droplets and wall films. They then separate into larger droplets at the edges of the disks and flow along the inner wall of the casing to the oil outlet. Gas with reduced oil mist is exhausted along the inner wall of the cyclone.

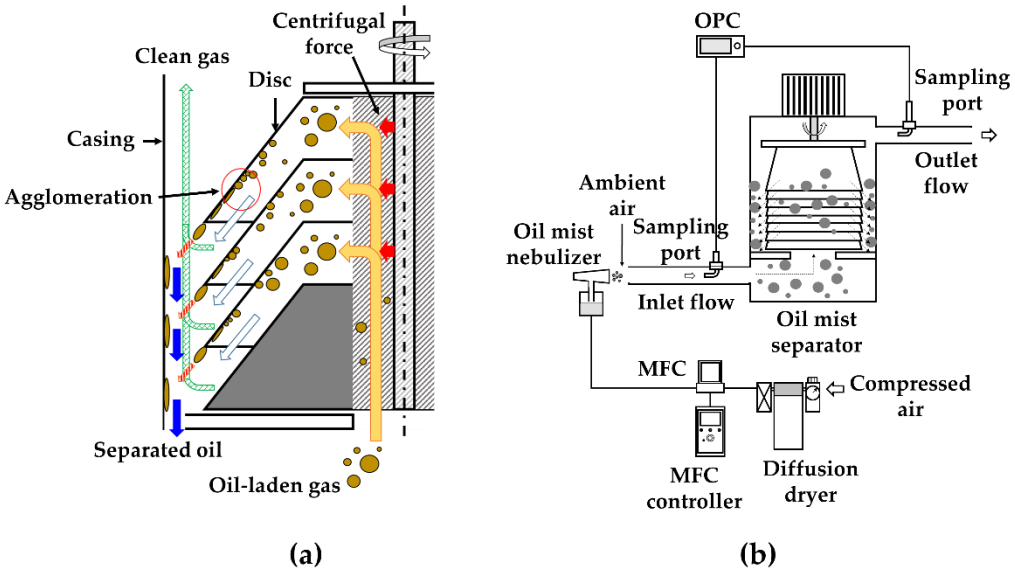


**Figure 3.** Schematics of: (**a**) disk-stack oil separator (showing the working principle); (**b**) experimental setup for performance testing.

Figure 3b shows a schematic of the experimental setup. Tapping oil (Speed Tap ST-501, ELE, Anseong, South Korea) was used to generate the oil mist, and the chemical composition of the oil provided by the manufacturer is shown in Table 2.

**Table 2.** Chemical composition of oil particles used in the experiment.

| Composition | Contents (%) |
|---|---|
| Propylene dichloride | 45~55 |
| Distillates (petroleum), hydrotreated light paraffinic | 35~45 |
| Distillates (petroleum), hydrotreated heavy paraffinic | |
| Sulfurized lard oil | 15~25 |
| 2,6-Di-tert-butyl-p-cresol | |
| extreme pressure additives | 5~0 |

These oil mists were generated by atomizing tapping oil using a pneumatic nebulizer (8900-7, Salter Labs, Walker, MI, USA). The operation of the pneumatic nebulizer requires a compressed gas supply. The compressed gas is delivered through a region of negative pressure created by the jet passing through the capillary tube. The liquid to be atomized is entrained in a gas stream and sheared into a liquid film. This film is unstable due to surface tension and breaks into droplets. A baffle installed inside the nebulizer serves to return the larger particles to the liquid reservoir and allow the atomized particles to escape. The droplet size produced by a nebulizer is determined by the properties of the solution (density, viscosity, surface tension) and the velocity of the gas. The velocity of the gas flow that induces atomization is a major determinant of the aerosol size, and

there is an inverse relationship between the droplet size and flow velocity due to the increased shear force at higher flow rates [40]. Because tapping oil was used for the liquid used in the experiment, the size of the generated particles was adjusted by controlling the amount of gas supplied to the nebulizer. Compressed air with 1.2 bar was delivered to a nebulizer at 3–4.3 L/min using a mass flow controller (MFC) (FC-2900, Mykrolis, Billerica, MA, USA). This MFC controls the flow with an accuracy of ±1.0% full scale. Transparent acrylic ducts were installed at the inlet and outlet of the separator to check the flow of the oil particles. The duct-flow velocity was measured using a multifunction instrument (Testo 480, Testo, Titisee-Neustadt, Germany), and the oil-particle concentrations were derived with an optical particle counter (OPC) (Grimm 1.109; Grimm Technologies, Ainring, Germany). The instruments used in the experiments were calibrated carefully by the manufacturer. Regarding the particle-concentration measurement, the OPC used in the experiment guarantees a measurement accuracy of ±5% based on the particle mass. Moreover, in the case of the Testo 480 device used to measure the flow velocity, it is possible to measure the flow velocity in the range from 0.6 to 40 m/s with a resolution of 0.2 m/s + 1%, and Testo 480 guarantees a measurement accuracy of ±0.1 m/s. The inlet was divided into three heights to measure the flow velocity at each point, and the particle concentration was measured by inserting a probe into the center of the inlet and outlet ducts. For each case, the particle concentration and flow rate were measured three times, and the uncertainty was expressed using the standard deviation of the measured values. The power consumption was logged using a digital power meter (WT333E, Yokogawa Electric, Tokyo, Japan). The digital power meter used in this experiment provides a basic power accuracy of ±0.15% (50/60 Hz) on all measurement ranges. The particle-removal efficiency was calculated using Equation (1):

$$\eta(\%) = (1 - \frac{C_{out}}{C_{in}}) \times 100 \quad (1)$$

where $\eta$ is the particle-removal efficiency (%), $C_{out}$ is the mass concentration of particles at the outlet of the separator (μg/m$^3$), and $C_{in}$ is the mass concentration of particles at the inlet (μg/m$^3$). As mentioned above, a pressure difference between the inlet and outlet develops during blade rotation, thereby inducing airflow. The inflow rate according to the blade rpm was measured. The theory underpinning this work is the semiempirical formula used by Lapple [41] to calculate $d_{pc}$, which is a measure of the theoretical removal efficacy of a conventional cyclone [41]:

$$d_{pc} = \left[\frac{9\mu W}{2\pi N_e V_i(\rho_p - \rho_p)}\right]^{1/2} \quad (2)$$

where $N_e$ is the effective number of turns; $V_i$ is the gas-inflow velocity (m/s); $\rho_p$ is the particle density (800 kg/m$^3$); $\rho_g$ is the gas density (1.176 kg/m$^3$); $\mu$ is the gas viscosity ($1.86 \times 10^{-5}$ kg/m·s); $W$ is the inlet width (0.003 m). The $d_{pc}$ is proportional to the square root of the gas viscosity and width of the inlet, and it is inversely proportional to the square root of the effective number of turns, inlet-gas velocity, and density difference between the particles and gas.

No published papers on the evaluation of the commercial centrifugal oil-mist collector for CNC machine tools were found. Therefore, we tested the commercial centrifugal oil-mist collector (Filtermist S800, Filtermist, Telford, UK), which is the most widely available on the Korean market, and we compared it with the oil-mist cyclone in this study. The commercial centrifugal oil-mist collector was operated under the rated operation condition at 3350 rpm, 660 W.

## 3. Results and Discussion

Figure 4 shows the flow rate according to the shape of the rotor blade and disks. As the rpm increased, so too did the pressure difference between the front/rear ends of the disks, which, in turn, linearly increased the flow rate. When the least powerful (120 W)

motor was used at 3500 rpm, the flow rate was 1.10 $m^3$/min when the rotor blades shown in Figure 2a were employed. However, when regular and/or cone-shaped disks were attached to the rotor blades, the flow rate decreased to 0.98 and 0.85 $m^3$/min, respectively, because the outlet flow rate instantaneously increased when disks were added, while the flow rate decreased because the airflow through the disks was disturbed. At the same rpm values, the flow rate associated with the cone-shaped disks was lower than that associated with the regular disks, which is because of the pressure drop caused by a sudden change in direction of the air streamline when the disks were aligned diagonally downward. The maximum speed of the 120 W motor is only 3500 rpm, and we thus used 750 W and 1.5 kW motors to handle higher flow rates (i.e., more pollutants). As the motor output increased from 120 to 750 W, the motor rotation speed and flow rate increased linearly from 3500 to 6500 rpm, and the flow rate of 0.85 $m^3$/min at 3500 rpm rose to 1.34 $m^3$/min at 6500 rpm. Although the power consumption increased 6.3-fold for the same geometries, the resolution and flow rates increased approximately 2-fold. Thus, to enhance the flow rate, the blade and cone disk sizes were increased. When the 1.5 kW motor was used, the rotor diameter increased from 80 to 130 mm (Case 5). The inflow flow rate was 1.43 $m^3$/min at 2000 rpm, 2.21 $m^3$/min at 3000 rpm, 2.96 $m^3$/min at 4000 rpm, and 3.73 $m^3$/min at the maximum rotational speed of 5000 rpm. In addition, compared with the use of a 750 W motor (Case 4), the flow rate increased 3.0-fold at 2000 rpm, and 3.5-fold at 5000 rpm (i.e., at the same rpm values). When the power consumption of the motor doubled, the flow rate increased more than 3-fold at the same rpm values, indicating that the flow rate was more affected by the separator geometry than in Cases 3 and 4.

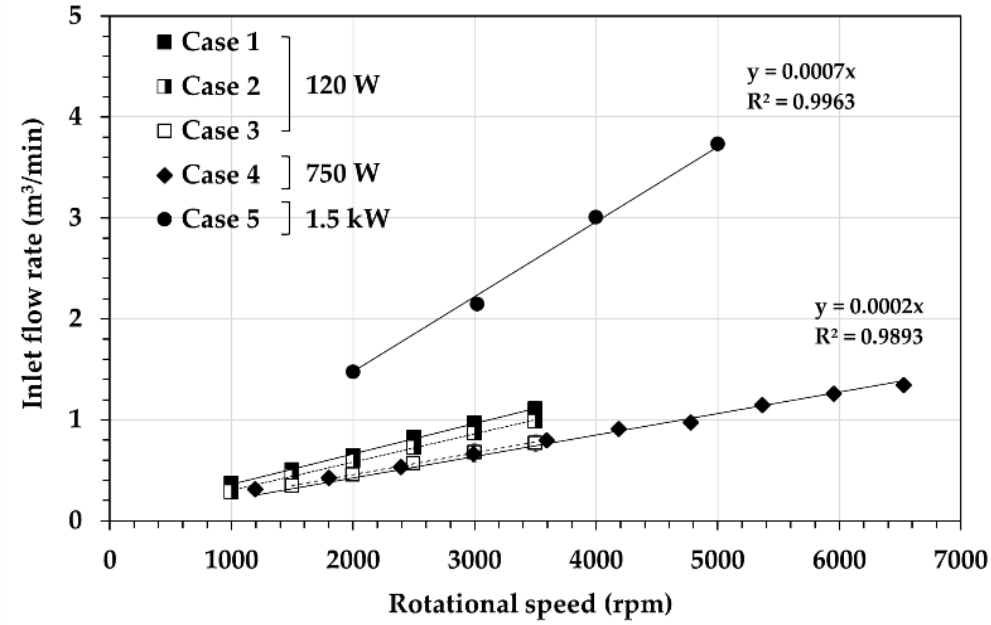


**Figure 4.** Separator flow rate with changes in disk shape and rpm.

Figure 5a shows the mass-concentration distribution according to the oil-particle size, as measured at the inlet side of the separator. The mass concentration of oil particles (total suspended particles (TSPs)) passing through the inlet was maintained at 33 mg/$m^3$ by adjusting the airflow rate into the nebulizer. The particle concentrations decreased for particles 0.6–0.7 μm in diameter; the highest concentrations were evident for particles 3–5 μm in diameter. Figure 5b shows the penetration rates of $PM_{10}$ oil particles according to disk shape at 3500 rpm. The penetration rate was 98.95% when a rotor blade without disks was used (Figure 1a), but it was only 68.8% when a flat disk was attached to the blade (Figure 1b); this represents a 30.5% improvement compared with the diskless cyclone separator. However, the cyclone with a cone-shaped disk (Figure 2a) removed 81.5% of $PM_{10}$ (the penetration was thus 18.5%); this constituted a 73.1% improvement compared

with the device with a flat disk. As disks were added to the blade, the velocity at which the particles passing through the disks collided with the wall increased, enhancing the removal efficiency. Although flow-rate differences developed during high-speed rotation (when the stream direction changed because of changes in disk shape), the streamline formed in the direction opposite to the exit angle of the cyclone when cone-shaped disks were employed, and the oil-collection efficiency, then rapidly increased. Therefore, the use of a cone-shape geometry significantly increases the removal of particles < 10 μm in diameter, even though that geometry slightly decreases the flow rate.

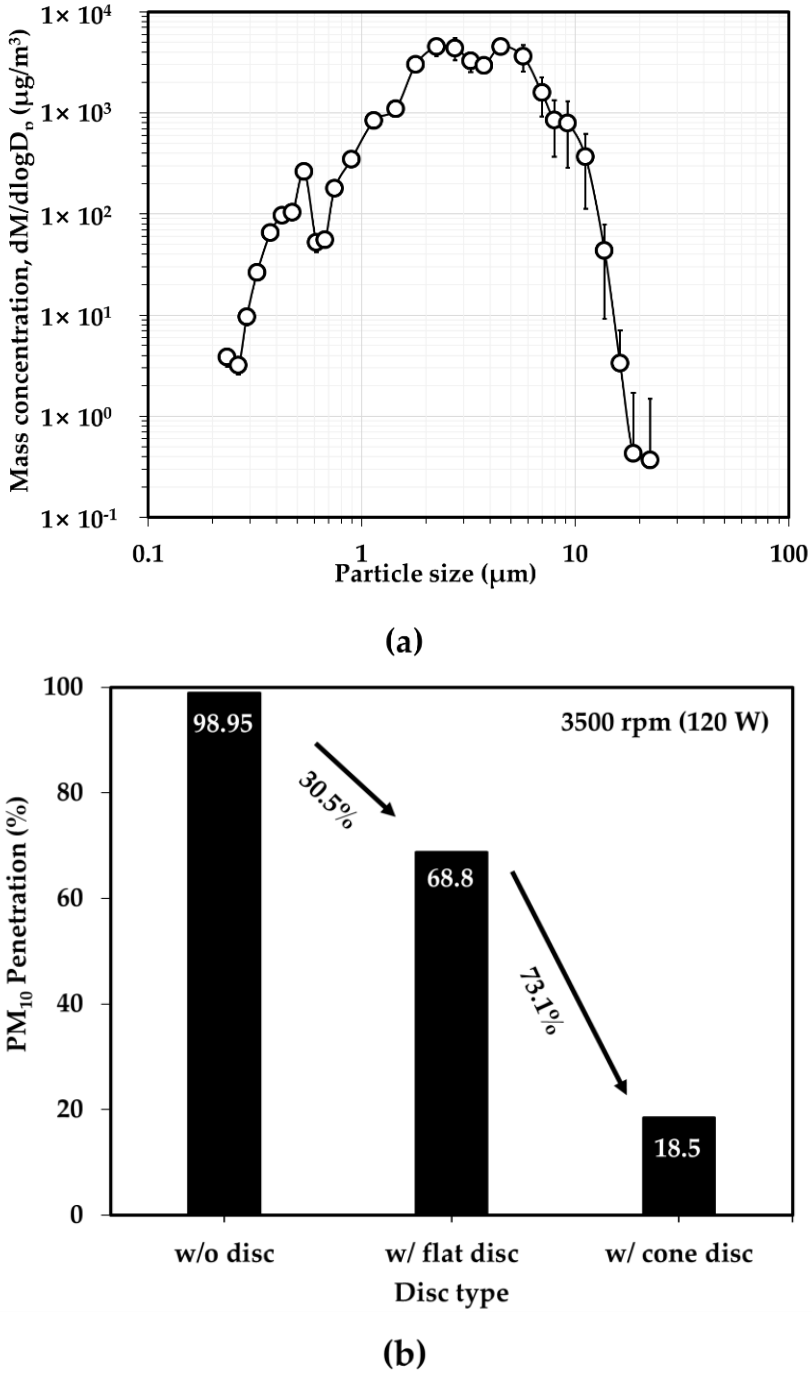


**Figure 5.** (**a**) Oil-mist mass concentrations at the inlet according to particle size. (**b**) Penetration rates of $PM_{10}$ particles at 3500 rpm (120 W) for different disk shapes.

Figure 6a shows the oil-particle-removal efficiency according to the rotational speed and flow rate. As shown in Figure 6a, when a 750 W motor and 80 mm rotor blades were operated at an rpm of 6000 (1.26 $m^3$/min), ≥95% of oil particles with a diameter of 2–10 μm were removed, but the particle-collection efficiency decreased with the particle size. As the rpm increased, so too did the centrifugal force applied to the oil particles, and the particle-collection efficiency was enhanced. When the rpm was 6000 (1.26 $m^3$/min), the diameter $d_{pc}$ associated with 50% oil-particle removal was about 1.08 μm; the $d_{pc}$ increased to about 1.60 μm as the rpm fell to 2500 rpm (0.57 $m^3$/min).

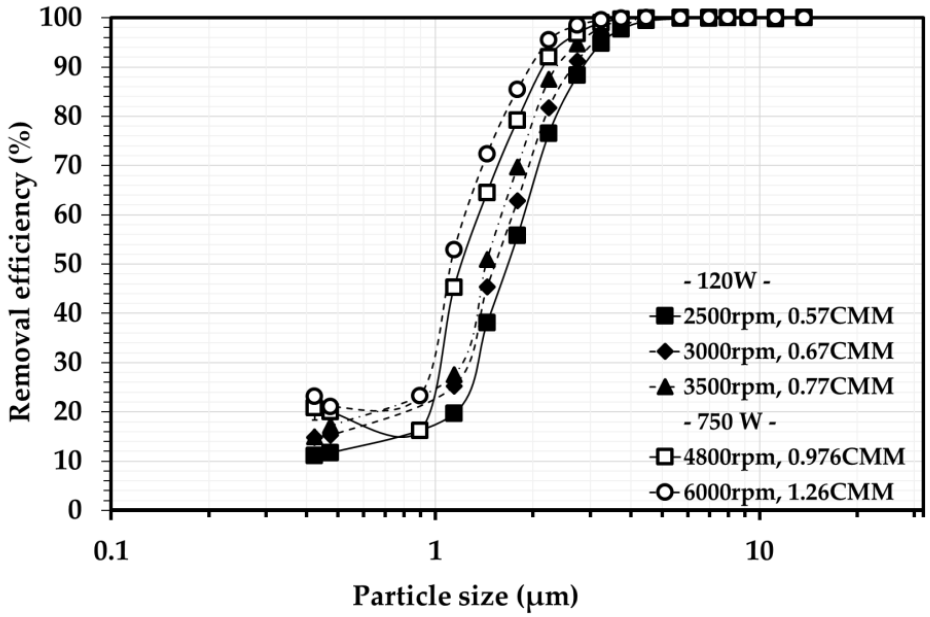


(a)

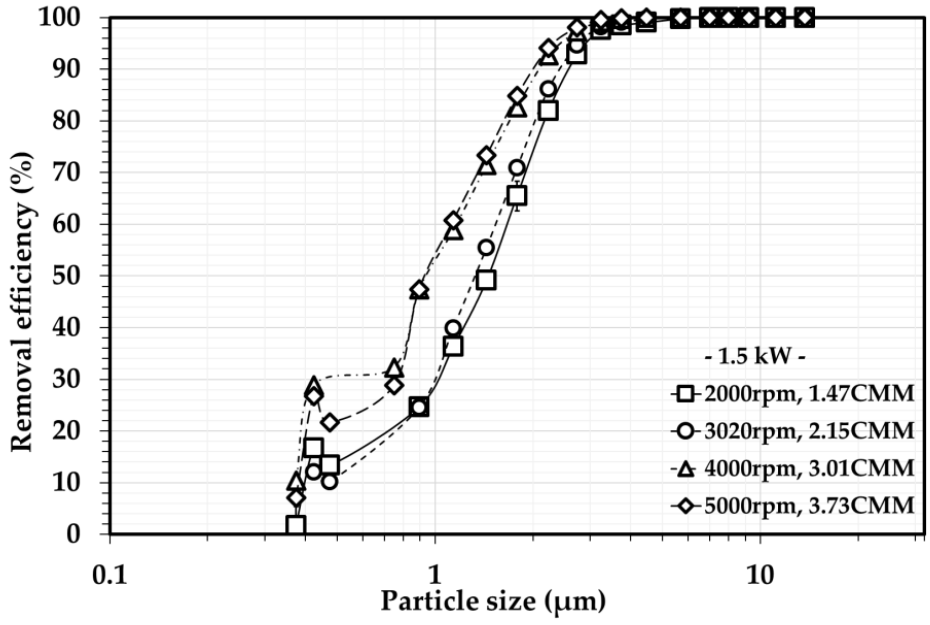


(b)

**Figure 6.** *Cont.*

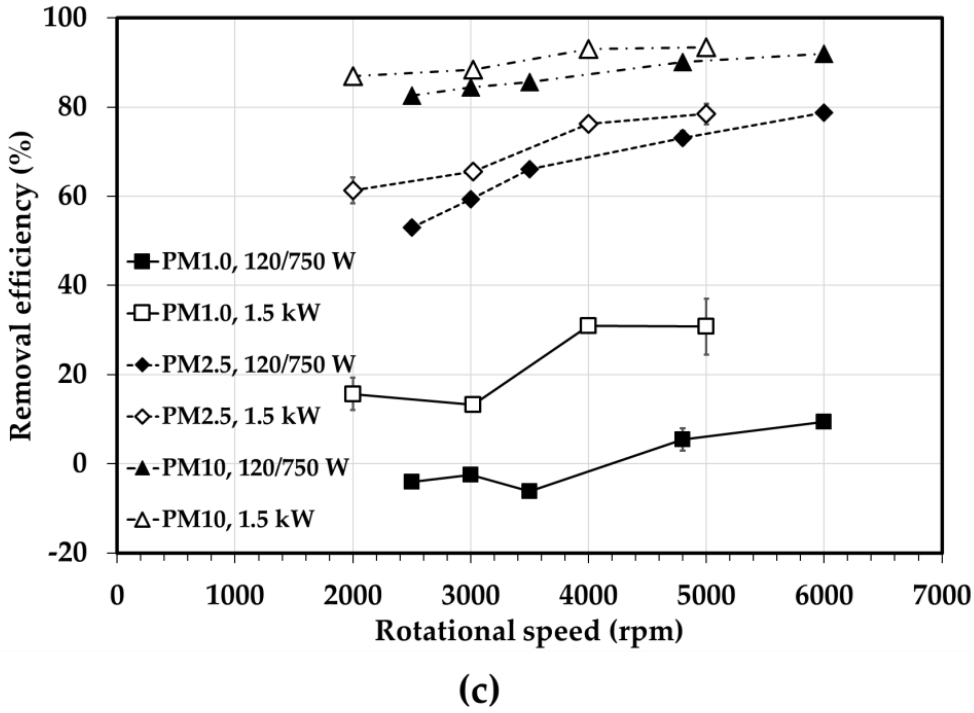


**Figure 6.** Oil-mist-removal efficiencies according to rpm: (**a**) 120 W motor; (**b**) 1.5 kW motor; (**c**) $PM_{1.0}$, $PM_{2.5}$, and $PM_{10}$ removal efficiencies at different rpm values.

Similarly, as shown in Figure 6b, when a 1.5 kW motor and 130 mm rotor blades were used at 5000 rpm (3.73 $m^3$/min), the $d_{pc}$ was about 0.94 μm; when the rpm was reduced to 2000, the $d_{pc}$ increased to about 1.47 μm. The theoretical evaluation of a separator in which the particle-collection efficiency is affected by centrifugal force requires the calculation of the $d_{pc}$ using Equation (2); the $d_{pc}$ is inversely proportional to the square root of the rpm. The $d_{pc}$ was indeed inversely proportional to the rpm. Han et al. [42] explored the behavior of oil particles according to the rpm of a cyclone with rotary blades. When the rpm was low, the flow rate (from inlet to outlet) was greater than the rotational flow, and the oil mist moved with the flow to become concentrated near the outlet [42]. However, when the rpm was (considerably) increased, oil mist also collected near the wall after passage through the rotor inlet. Moreover, the flow velocity was increased with the rpm. As the centrifugal force and number of particles colliding with the wall increase, the particle-collection efficiency increases and the $d_{pc}$ falls.

Figure 6c shows the removal efficiencies of $PM_{10}$, $PM_{2.5}$, and $PM_{1.0}$ according to the change in rpm. When using a 750 W motor and an 80 mm blade, the removal efficiencies of $PM_{10}$, $PM_{2.5}$, and $PM_{1.0}$ were 92.0%, 78.8%, and 9.4%, respectively, as the rotation speed increased to 6000 rpm. The $PM_{1.0}$-removal efficiency was lower than those of $PM_{10}$ and $PM_{2.5}$; in particular, when the rpm was ≤3500 rpm, the $PM_{1.0}$-removal efficiency was negative, which is probably because the $PM_{1.0}$ was increased by the breakup of larger particles, rendering the concentration at the outlet higher than the concentration at the inlet. To ensure efficient $PM_{1.0}$ removal, the separator must operate at >3500 rpm. Using a 1.5 kW motor and a 130 mm blade increased the PM-removal efficiency at the same rpm depending on the blade size. At 5000 rpm, the removal efficiencies of $PM_{10}$, $PM_{2.5}$, and $PM_{1.0}$ were 93.4%, 78.4%, and 30.7%, respectively. In terms of the TSP-removal efficiency, as shown in Figure 5a, it was only about 1% different from that of $PM_{10}$ because there were few particles with a diameter greater than 10 μm.

Because no published papers on the performance evaluation of the commercial centrifugal oil-mist eliminator for CNC machine tools were found, we tested the commercial centrifugal oil-mist collector (Filtermist S800, Filtermist, Telford, UK), which is the most widely available on the Korean market, and we compared it with the oil-mist cyclone

in this study. The test results of the commercial centrifugal oil-mist collector showed a $PM_{10}$-removal efficiency of 97.8% under the rated operating conditions of 3350 rpm and 660 W.

The semi-empirical equation of Lapple [41] was used to calculate the $d_{pc}$ (which determines the theoretical removal efficiency of a conventional cyclone separator), and the effects of the rotational characteristics and inflow velocity on the oil-removal efficiency were explored [41].

Figure 7 shows the calculated flow velocities at the disk outlet according to the motor rpm. The flow rate between disks was calculated by dividing the rates at the front and rear ends by the area between adjacent disks. As the rpm increased, the inlet flow rate rose, as did the flow velocity out of the disk. The $d_{pc}$ of a conventional cyclone separator can be written as follows:

$$d_{pc} \propto \left[\frac{1}{N_e V_i}\right]^{\frac{1}{2}} \tag{3}$$

where $N_e$ is the effective number of turns, and $V_i$ is the gas-inflow velocity (m/s).

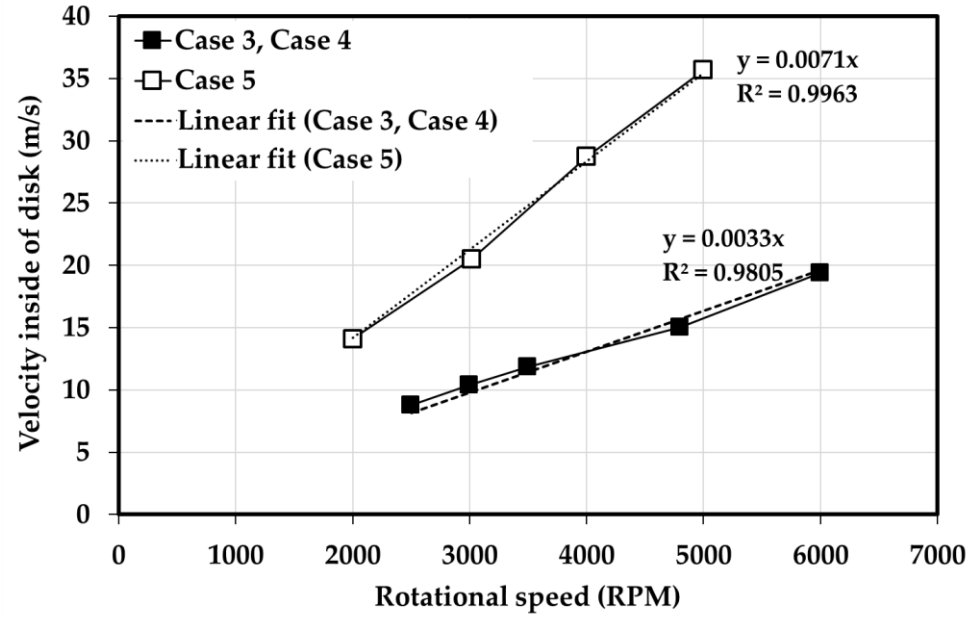


**Figure 7.** Flow velocities inside the disk according to the rpm.

According to Lapple (1951), the $d_{pc}$ of a conventional cyclone is inversely proportional to the square roots of the rotation speed and inlet flow velocity; however, for the oil-mist separator in this study, the $d_{pc}$ is inversely proportional to both the rotation speed and inlet flow velocity (Figure 8) [41]:

$$d_{pc} \propto \left[\frac{1}{N_e}\right] \propto \left[\frac{1}{V_i}\right], \; V_i = \alpha \times N_e \tag{4}$$

where $N_e$ is the effective number of turns, $V_i$ is the gas-inflow velocity (m/s), and $\alpha$ is proportionality constant.

As mentioned above, as the flow rate increased with the rpm, the oil-removal efficiency as the oil-removal capacity (mg/min) was calculated:

$$Removal\ capacity\ (\mathrm{mg/min}) = Q \times \eta \times C_{in} = Q \times (C_{in} - C_{out}) \tag{5}$$

where $\eta$ is the particle-removal efficiency according to particle size, $Q$ is the flow rate of the separator ($m^3$/min), $C_{in}$ is the particle mass concentration at the inlet ($\mu g/m^3$), and $C_{out}$ is the particle mass concentration at the outlet ($\mu g/m^3$).

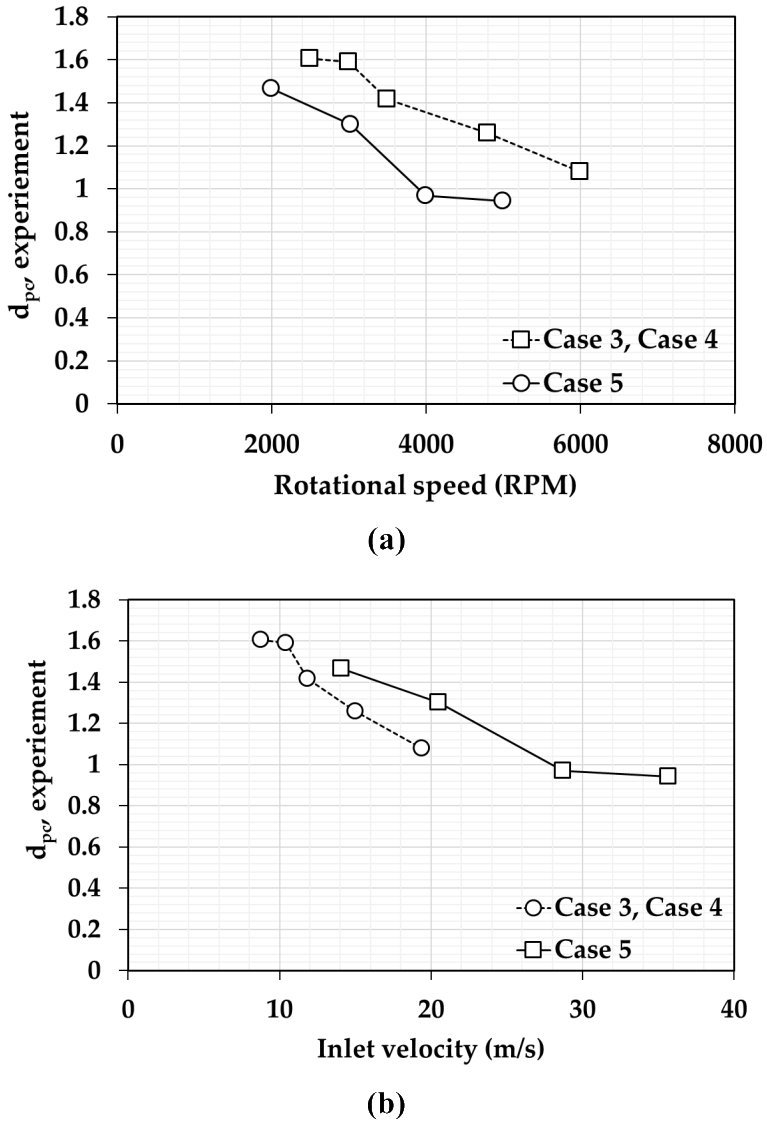


**Figure 8.** Experimental $d_{pc}$ values derived by reference to: (**a**) the rpm of the cyclone separator and (**b**) inlet velocity of the cyclone separator.

Figure 9 compares the reductions in the $PM_{1.0}$, $PM_{2.5}$, and $PM_{10}$ particle numbers according to the rpm. For $PM_{1.0}$, the concentration at the outlet was higher than at the inlet (attributable to particle breakup), yielding a maximum reduction of 1.4 mg/min, even when the rpm increased. For $PM_{2.5}$ particles (80 mm blades; 750 W motor), the rate of the oil-particle reduction increased from 3.15 to 12.0 mg/min as the rpm rose from 2500 to 6000. When 130 mm blades were used with a 1.5 kW motor, the reduction increased from 8.48 to 28.32 mg/min as the rpm rose from 2000 to 5000. For $PM_{10}$ particles, the reduction increased from 15.45 to 38.83 mg/min as the rpm rose from 2500 to 6000 when an 80 mm rotor blade was employed with a 750 W motor. When 130 mm rotor blades were used with a 1.5 kW motor, the reduction increased from 39.74 to 115.32 mg/min as the rpm rose from 2000 to 5000. The oil-particle removal rate/min increased linearly with the inlet flow rate. Figure 9 shows that when a 130 mm blade was combined with a 1.5 kW motor, the PM-reduction efficiency was lower (at low rpm) than when an 80 mm blade was used with a 750 W motor. The oil-reduction efficiency when using the 1.5 kW motor was always greater than that afforded by the 120 and 750 W motors, except when the 1.5 kW motor operated at 2000 rpm because the flow-rate difference exceeded the PM-reduction efficiency as the rpm increased.

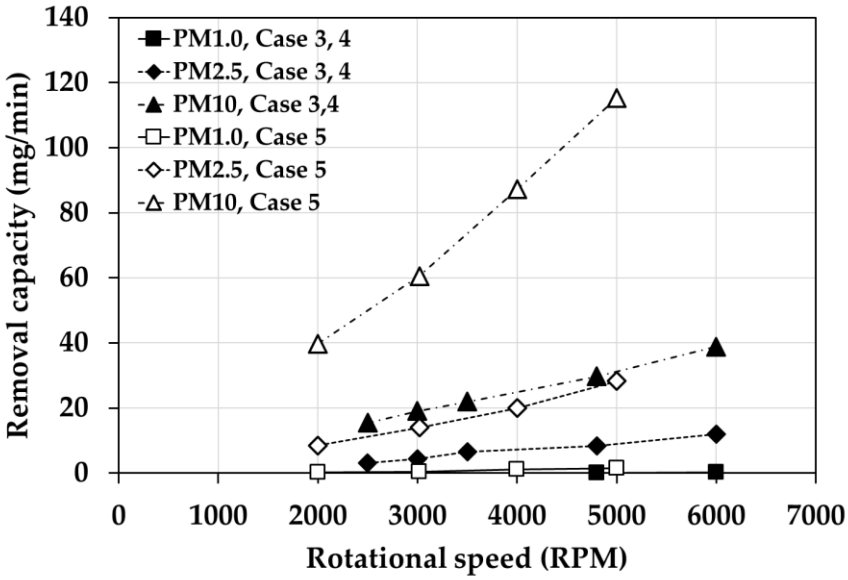


**Figure 9.** Oil-mist-removal capacity according to the rpm of the separator.

A graph of the cyclone efficiency versus the particle size is sometimes S-shaped; the curve can be approximated by the logistic Equation (6) (Iozia and Leith, 1990) [43]:

$$\eta = \frac{1}{1 + \left(d_{pc}/d_p\right)^{\beta}} \tag{6}$$

where $\eta$ is the cyclone efficiency according to particle size ($d_p$), $d_{pc}$ (μm) is the cut diameter of the particle, $d_p$ is the particle diameter (μm), and $\beta$ is the slope. In the logistic equation, the sharpness of the cyclone cut (maximum slope of the efficiency curve) increases with the slope (Equation (6)) and decreases in $d_{pc}$. Figure 10 shows the experimental particle-removal efficiency according to the particle diameter, and a graph of the predicted removal efficiencies for particles of all diameters derived using conventional models. First, the efficiency of the separator was calculated by substituting the experimental cut particle diameter into the semi-empirical equation of Lapple [41], which yields the efficiency for $\beta = 2$; the efficiency can be calculated using Equation (7) [41]:

$$\eta = \frac{1}{1 + \left(d_{pc}/d_p\right)^{2}} \tag{7}$$

where $\eta$ is the efficiency for a particle of size ($d_p$), $d_{pc}$ (μm) is the cut diameter of the particle, and $d_p$ is the particle diameter (μm). Figure 10 shows the experimental efficiency curve for particles of all sizes, and the theoretical efficiencies calculated using the Lapple [41] formula (Equation (7)); the latter is indicated as "Lapple" in the legend for Figure 10 [41]. For particles with a diameter greater than the $d_{pc}$, the theoretical efficiency is lower than the experimental one, thus yielding an efficiency curve that is not sharper than the experimental curve. The use of $\beta > 2$ prevents overprediction by the Lapple function for particles of a diameter < $d_{pc}$, and underprediction for other particles [41]. To obtain an appropriate $\beta$ value, Equation (6) was used. The result is shown in Figure 10. The graph marked "Model" in the legend for Figure 10 was derived using a logistic equation (i.e., Equation (6)). Iozia and Leith [43] employed the generalized distribution of Equation (6) to fit the experimental data for Stairmand cyclones, and for other cyclones with geometries that were variations of the basic Stairmand design [43]. They reported that the $\beta$ ranged from 2.77 to 5.22. Thus, a $\beta$ was suggested that is 2–6 for most industrial cyclones. The $\beta$ for the authors' separator was calculated to be 4, which is consistent with the suggestion above.

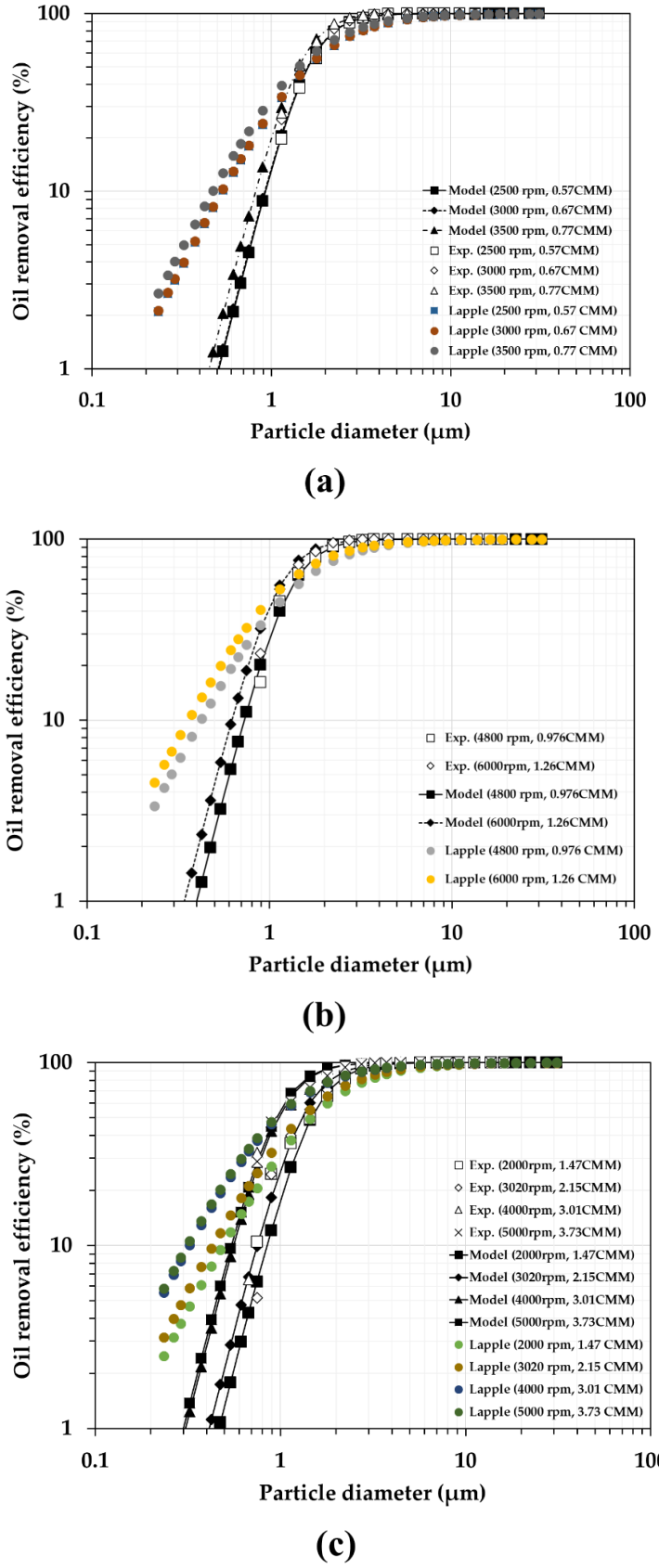


**Figure 10.** Experimental oil-removal efficiencies and approximate theoretical efficiencies derived using the Lapple and logistic equations: (**a**) cyclone with 120 W motor, (**b**) cyclone with 750 W motor, (**c**) cyclone with 1.5 kW motor.

## 4. Conclusions

Because the inhalation of oil mist by workers adversely affects their health, regulations and studies to reduce workers' exposure to oil mist have been actively conducted. Although there are methods such as ventilation and wearing personal protective equipment to reduce the exposure of workers to oil mist, it is also important to remove the oil mist generated from machine tools. The ability of a rotational cyclone to capture particles < 10 μm in diameter for varied geometries, powers, airflow velocities, and rpm was assessed. Oil-mist particles (mass concentration of ~30 mg/m$^3$; mostly < 10 μm in diameter) were generated by an atomizer, and the removal efficiency was measured by an optical particle counter. Experimentally, the airflow rate increased linearly with the number of rotations of the rotor blades. At the same rpm and power consumption, the diskless cyclone showed the lowest efficiency, and the mist-removal efficiency was greatly improved when the flat disk and cone-shaped disk were added; however, the airflow rate decreased as the disks were added. When a 750 W motor and 80 mm rotor blades were operated at an rpm of 6000 (1.26 m$^3$/min), ≥95% of the oil particles with diameters of 2–10 μm were removed. As the rpm increased, so too did the centrifugal force applied to the oil particles, and the removal efficiency was enhanced. When the rpm was 6000 (1.26 m$^3$/min), the $d_{pc}$ was about 1.08 μm; the $d_{pc}$ increased to about 1.60 μm as the rpm fell to 2500 rpm (0.57 m$^3$/min). Similarly, when a 1.5 kW motor and 130 mm rotor blades were used at 5000 rpm (3.73 m$^3$/min), the $d_{pc}$ was about 0.94 μm; when the rpm was reduced to 2000, the $d_{pc}$ increased to about 1.47 μm. Even if the oil-mist-removal efficiency is high, if the flow rate that the cyclone can handle is low, then the amount of oil mist that can be removed per hour will be reduced, and it will take more time to remove the oil mist inside the machine tool. Therefore, the oil-mist-removal capacity is important. When the 130 mm rotor blade and 1.5 kW motor were combined, the PM-reduction efficiency was lower than the cyclone with an 80 mm blade and 750 W motor, but the higher oil-removal capacity was due to the higher flow rate. Thus, the oil-removal capacity was predominantly affected by the geometry of the cyclone rather than the rpm. Finally, the experimental data were approximated using a logistic equation; the slope parameter (obtained by fitting) was 4, which was higher than that derived when the Lapple equation was employed to derive the efficiency curve.

In South Korea, it is estimated that the number of companies handling metalworking fluids in Korea for workplaces with five or more employees is 17,000. This corresponds to 13% of all chemical-handling companies, and at least 80,000 workers are exposed to the risk of metalworking fluids. In conventional rotating-drum centrifugal mist collectors, the filter still needs to be replaced frequently because contaminants are removed by the rotating drum and the drum's pad, acting as a filter. The oil-mist cyclone of this study is expected to contribute to the reduction in problems, such as secondary-pollutant generation and additional costs through frequent filter replacement, as the mist-removal efficiency is increased through a cone-shaped disk without using a filter.

**Author Contributions:** Funding acquisition, H.-J.K.; Project administration, H.-J.K.; Supervision, Y.L., Y.-J.K., B.H. and H.-J.K.; Validation, Y.L., Y.-J.K. and B.H.; Writing—original draft, H.L. All authors have read and agreed to the published version of the manuscript.

**Funding:** This work was supported by the Korea Institute of Energy Technology Evaluation and Planning (KETEP) and the Ministry of Trade, Industry & Energy (MOTIE) of the Republic of Korea (No. 20181110200170).

**Institutional Review Board Statement:** Not applicable.

**Informed Consent Statement:** Not applicable.

**Data Availability Statement:** Not applicable.

**Conflicts of Interest:** The authors declare no conflict of interest.

## Nomenclature

| | |
|---|---|
| MWF | Metalworking fluids |
| OSHA | Occupational Safety and Health Administration |
| PEL | Permissible exposure limits |
| TWA | Time-weighted average |
| CNC | Computer numerical control |
| ESP | Electrostatic precipitators |
| HEPA | High-efficiency particulate air |
| MFC | Mass flow controller |
| OPC | Optical particle counter |
| RPM | Revolution per minute |
| TSP | Total suspended particles |
| $PM_{10}$ | Particulate matter 10 |
| $PM_{2.5}$ | Particulate matter 2.5 |
| $PM_{1.0}$ | Particulate matter 1.0 |
| CMM | $m^3$/min |

## References


1. Wang, F.; Li, Z.; Wang, P.; Zhang, R. Experimental study of oil particle emission rate and size distribution during milling. *Aerosol Sci. Technol.* **2018**, *52*, 1308–1319. [CrossRef]
2. Wang, Y.; Murga, A.; Long, Z.; Yoo, S.J.; Ito, K. Experimental study of oil mist characteristics generated from minimum quantity lubrication and flood cooling. *Energy Built Environ.* **2021**, *2*, 45–55. [CrossRef]
3. Brinksmeier, E.; Meyer, D.; Huesmann-Cordes, A.G.; Herrmann, C. Metalworking fluids—Mechanisms and performance. *CIRP Ann.* **2015**, *64*, 605–628. [CrossRef]
4. Michalek, D.J.; Hii, W.W.S.; Sun, J.; Gunter, K.L.; Sutherland, J.W. Experimental and analytical efforts to characterize cutting fluid mist formation and behavior in machining. *Appl. Occup. Environ. Hyg.* **2003**, *18*, 842–854. [CrossRef] [PubMed]
5. Yacher, J.M.; Heitbrink, W.A.; Burroughs, G.E. Mist control at a machining center, part 2: Mist control following installation of air cleaners. *AIHAJ* **2000**, *61*, 282–289. [CrossRef]
6. Yue, Y.; Sun, J.; Gunter, K.L.; Michalek, D.J.; Sutherland, J.W. Character and behavior of mist generated by application of cutting fluid to a rotating cylindrical workpiece, part 1: Model development. *J. Manuf. Sci. Eng.* **2004**, *126*, 417–425. [CrossRef]
7. Heitbrink, W.A.; Evans, D.E.; Peters, T.M.; Slavin, T.J. Characterization and mapping of very fine particles in an engine machining and assembly facility. *J. Occup. Environ. Hyg.* **2007**, *4*, 341–351. [CrossRef]
8. Chen, Z.; Wong, K.; Li, W.; Liang, S.Y.; Stephenson, D.A. Cutting fluid aerosol generation due to spin-off in turning operation: Analysis for environmentally conscious machining. *J. Manuf. Sci. Eng.* **2001**, *123*, 506–512. [CrossRef]
9. Sheehan, M.J. *Final Report of the OSHA Metalworking Fluids Standards Advisory Committee*; US Department of Labor, Occupational Safety and Health Administrations: Washington, DC, USA, 1999.
10. Koh, D.H.; Park, J.H.; Lee, S.G.; Kim, H.C.; Choi, S.; Jung, H.; Kim, I.; Park, D. Development of Korean CARcinogen EXposure: An Initiative of the Occupational Carcinogen Surveillance System in Korea. *Ann. Work Expo. Health* **2021**, *65*, 528–538. [CrossRef]
11. Lillienberg, L.; Andersson, E.M.; Järvholm, B.; Torén, K. Respiratory symptoms and exposure–response relations in workers exposed to metalworking fluid aerosols. *Ann. Occup. Hyg.* **2010**, *54*, 403–411. [CrossRef]
12. Metalworking Fluids: Safety and Health Best Practices Manual. Available online: https://www.osha.gov/metalworking-fluids/manual (accessed on 10 June 2022).
13. Liu, R.; Ji, D.; Zhou, G.; Liu, Z.; Xu, Q.; Ramakrishna, S. Electrospun nanofibers for personal protection in mines. *Chem. Eng. J.* **2020**, *404*, 126558. [CrossRef]
14. Rubio-Romero, J.C.; del Carmen Pardo-Ferreira, M.; Torrecilla-García, J.A.; Calero-Castro, S. Disposable masks: Disinfection and sterilization for reuse, and non-certified manufacturing, in the face of shortages during the COVID-19 pandemic. *Saf. Sci.* **2020**, *129*, 104830. [CrossRef] [PubMed]
15. Roberge, R.J.; Coca, A.; Williams, W.J.; Powell, J.B.; Palmiero, A.J. Physiological impact of the N95 filtering facepiece respirator on healthcare workers. *Respir. Care* **2010**, *55*, 569–577. [PubMed]
16. Monjezi, M.; Jamaati, H. The effects of face mask specifications on work of breathing and particle filtration efficiency. *Med. Eng. Phys.* **2021**, *98*, 36–43. [CrossRef]
17. Roberge, R.J.; Bayer, E.; Powell, J.B.; Coca, A.; Roberge, M.R.; Benson, S.M. Effect of exhaled moisture on breathing resistance of N95 filtering facepiece respirators. *Ann. Occup. Hyg.* **2010**, *54*, 671–677. [CrossRef]
18. Lee, H.P.; Wang, D.Y. Objective assessment of increase in breathing resistance of N95 respirators on human subjects. *Ann. Occup. Hyg.* **2011**, *55*, 917–921. [CrossRef]
19. Lim, E.C.H.; Seet, R.C.S.; Lee, K.H.; Wilder-Smith, E.P.V.; Chuah, B.Y.S.; Ong, B.K.C. Headaches and the N95 face-mask amongst healthcare provsiders. *Acta Neurol. Scand.* **2006**, *113*, 199–202. [CrossRef]

20. Smith, C.L.; Whitelaw, J.L.; Davies, B. Carbon dioxide rebreathing in respiratory protective devices: Influence of speech and work rate in full-face masks. *Ergonomics* **2013**, *56*, 781–790. [CrossRef]
21. Hopkins, S.R.; Stickland, M.K.; Schoene, R.B.; Swenson, E.R.; Luks, A.M. Effects of surgical and FFP2/N95 face masks on cardiopulmonary exercise capacity: The numbers do not add up. *Clin. Res. Cardiol.* **2020**, *109*, 1605–1606. [CrossRef]
22. Sokolović, D.S.; Höflinger, W.; Sokolović, R.M.Š.; Sokolović, S.M.; Sakulski, D. Experimental study of mist generated from metalworking fluids emulsions. *J. Aerosol Sci.* **2013**, *61*, 70–80. [CrossRef]
23. Sutherland, J.W.; Kulur, V.N.; King, N.C.; Von Turkovich, B.F. An experimental investigation of air quality in wet and dry turning. *CIRP Ann.* **2000**, *49*, 61–64. [CrossRef]
24. Pan, Z.D.; Zhang, L.Z.; Zhao, J.J. Present situation of welding chimney pollution and the treatment technology. *Sci. Technol. Baotou Steel (Group) Corp.* **2007**, *4*, 77–79.
25. Wei, G.; Chen, B.; Lai, D.; Chen, Q. An improved displacement ventilation system for a machining plant. *Atmos. Environ.* **2020**, *228*, 117419. [CrossRef]
26. Vincent, J.H. *Aerosol Science for Industrial Hygienists*, 1st ed.; Elsevier: Amsterdam, The Netherlands, 1955; pp. 347–360. [CrossRef]
27. Kolb, H.E.; Kasper, G. Mist filters: How steady is their "steady state"? *Chem. Eng. Sci.* **2019**, *204*, 118–127. [CrossRef]
28. Wei, X.; Zhou, H.; Chen, F.; Wang, H.; Ji, Z.; Lin, T. High-efficiency low-resistance oil-mist coalescence filtration using fibrous filters with thickness-direction asymmetric wettability. *Adv. Funct. Mater.* **2019**, *29*, 1806302. [CrossRef]
29. Mead-Hunter, R.; King, A.J.; Mullins, B.J. Aerosol-mist coalescing filters—A review. *Sep. Purif. Technol.* **2014**, *133*, 484–506. [CrossRef]
30. Manzo, G.M.; Wu, Y.; Chase, G.G.; Goux, A. Comparison of nonwoven glass and stainless steel microfiber media in aerosol coalescence filtration. *Sep. Purif. Technol.* **2016**, *162*, 14–19. [CrossRef]
31. Chen, F.; Ji, Z.; Qi, Q. Effect of pore size and layers on filtration performance of coalescing filters with different wettabilities. *Sep. Purif. Technol.* **2018**, *201*, 71–78. [CrossRef]
32. Wei, X.; Chen, F.; Wang, H.; Zhou, H.; Ji, Z.; Lin, T. Efficient removal of aerosol oil-mists using superoleophobic filters. *J. Mater. Chem.* **2018**, *6*, 871–877. [CrossRef]
33. Zhang, J.; Pan, W.; Long, Z.; Wang, C.; Feng, Z. Study of the oil mist filtration performance: Pressure drop characteristics and filter efficiency model. *Aerosol Air Qual. Res.* **2017**, *17*, 1063–1072. [CrossRef]
34. Li, S.; Zhang, S.; Pan, W.; Long, Z.; Yu, T. Experimental and theoretical study of the collection efficiency of the two-stage electrostatic precipitator. *Powder Technol.* **2019**, *356*, 1–10. [CrossRef]
35. Zheng, C.; Liang, C.; Liu, S.; Yang, Z.; Shen, Z.; Guo, Y.; Zhang, Y.; Gao, X. Balance and stability between particle collection and re-entrainment inawide temperature-range electrostatic precipitator. *Powder Technol.* **2018**, *340*, 543–552. [CrossRef]
36. Yawootti, A.; Intra, P.; Tippayawong, N.; Rattanadecho, P. An experimental study of relative humidity and air flow effects on positive and negative corona discharges in a corona-needle charger. *J. Electrost.* **2015**, *77*, 116–122. [CrossRef]
37. Said, H.; Aissou, M.; Nouri, H.; Zebboudj, Y. Analysis of the Current-Voltage Characteristic during the Corona Discharge in Wires-To-Planes Electrostatic Precipitator under Variable Air Humidity. *Acta Phys. Pol. A* **2019**, *135*, 320–325. [CrossRef]
38. Zhang, S.; Pan, W.; Zhang, H.; Long, Z.; Yu, T. High-efficient removal of airborne oil mist in a wire-plate electrostatic precipitator. *J. Electrost.* **2020**, *108*, 103516. [CrossRef]
39. Mist-Collection-of-Metalworking-Fluids. Available online: https://www.donaldson.com/content/dam/donaldson/dust-fume-mist/literature/north-america/industries-markets/f118000/Mist-Collection-of-Metalworking-Fluids.pdf (accessed on 20 August 2022).
40. Hess, D.R. Nebulizers: Principles and performance. *Respir. Care* **2000**, *45*, 609.
41. Lapple, C.E. Processes use many collection types. *Chem Eng.* **1951**, *58*, 144–151.
42. Han, J.H.; Ma, S.J. Trajectory characteristics of liquid drops inside the cyclone of an air cleaner. In Proceedings of the KSME 2010 Autumn Conference, Phoenixpark, Pyeongchang, 11–14 May 2010; pp. 3401–3403.
43. Iozia, D.L.; Leith, D. The logistic function and cyclone fractional efficiency. *Aerosol Sci. Technol.* **1990**, *12*, 598–606. [CrossRef]